Available online at www.sciencedirect.com
ScienceDirect
Journal of Computational Physics 227 (2008) 4853–4872
JOURNAL OF COMPUTATIONAL PHYSICS
www.elsevier.com/locate/jcp

On entropy generation and dissipation of kinetic energy in high-resolution shock-capturing schemes ☆

B. Thornber [a], D. Drikakis [a,*], R.J.R. Williams [b], D. Youngs [b]

[a] *Fluid Mechanics and Computational Science Group, Aerospace Sciences Department, School of Engineering, Cranfield University, Cranfield MK43 0AL, United Kingdom*
[b] *AWE, Aldermaston, United Kingdom*

Received 25 April 2007; received in revised form 26 December 2007; accepted 14 January 2008
Available online 2 February 2008

Abstract

This paper addresses entropy generation and the corresponding dissipation of kinetic energy associated with high-resolution, shock-capturing (Godunov) methods. Analytical formulae are derived for the rate of increase of entropy given arbitrary jumps in primitive variables at a cell interface. It is demonstrated that for general continuously varying flows the inherent numerical entropy increase of Godunov methods is not proportional to the velocity jump cubed as is commonly assumed, but it is proportional to the velocity jump squared. Furthermore, the dissipation of kinetic energy is directly linked to temperature multiplied by change in entropy at low Mach numbers. The kinetic energy dissipation rate is shown to be proportional to the velocity jump squared and the speed of sound. The leading order dissipation rate associated with jumps in pressure, density and shear waves is detailed and further shown that at low Mach number it is the dissipation due to the perpendicular velocity jumps which dominates. This explains directly the poor performance of Godunov methods at low Mach numbers. The analysis is also applied to high-order accurate methods in space and time and all analytical results are validated with simple numerical experiments.

Keywords: High-resolution methods; Godunov methods; Dissipation; Kinetic energy; Entropy; Large eddy simulation; Low Mach number

1. Introduction

The finite volume (FV) high-resolution, shock-capturing methods (henceforth labelled as Godunov methods) have proven extremely successful in the simulation of high-speed flows and is an essential tool in many applications in the broader field of compressible fluid dynamics. The Euler equations can form steep discontinuities in compressible flows and in order to provide a stable and non-oscillatory solution a certain level of

☆ Contains material © British Crown Copyright 2006/MOD.

* Corresponding author. Tel.: +44 1234 754796; fax: +44 1234 752149.
E-mail address: d.drikakis@cranfiled.ac.uk (D. Drikakis).

0021-9991/$ - see front matter © 2008 Elsevier Inc. All rights reserved.
doi:10.1016/j.jcp.2008.01.035

artificial dissipation is added to the solution. In a Godunov method this dissipation is added through the upwind behaviour of the numerical scheme. Unfortunately, the numerical dissipation required to stabilise the solution also causes anomalous increase in entropy, and corresponding dissipation of kinetic energy. The aim of this paper is to understand the rate of dissipation of kinetic energy and rate of entropy increase. These are issues especially important in describing the poor performance of Godunov methods in simulations of low Mach number flows; determining the implicit subgrid model for implicit large eddy simulations (ILES); and in eliminating entropy errors associated with unsteady flow features. Issues such as convergence problems and difficulties due to round off errors are not dealt with in this paper, for further information see for example [1,2] and references within.

Several previous papers have discussed the influence of artificial viscosity on the simulation of inviscid flows, primarily applied to finite difference methods. Noh [3] detailed the behaviour of finite difference schemes, highlighting the sometimes undesirable effects of the von Neumann and Richtmyer type viscosity when simulating strong shock waves due to the overly dissipative nature of certain formulations, especially in the absence of heat conduction. Christensen [4] draws parallels between the dissipation inherent in a Godunov method and that due to artificial viscosity method. The different forms of artificial viscosity are further discussed in Benson [5] with respect to their performance in capturing shock waves. Volpe [6] demonstrated using several numerical examples that FV methods provide inaccurate results at low Mach number flows due to excess numerical dissipation. Later, Menikoff [7] noted that artificial viscosity is responsible for the entropy errors associated with a diffused shock and that this error does not disappear with mesh refinement. This type of entropy error is commonly referred to as 'wall heating' in the literature. Several papers by Guillard [8,9,1] examine the low Mach number problem, demonstrating that at low Mach numbers the artificial viscosity present in Godunov schemes leads to an undesirable scaling of the pressure with respect to the Mach number (in the absence of acoustic waves) and proposing a form of preconditioning of the governing equations to correct this. However, to the authors knowledge, an analytical form of entropy generation and dissipation of kinetic energy in Godunov schemes has not been yet been derived. This paper details the first validated analytical description of the dissipation of kinetic energy in Godunov methods.

Two factors have increased the importance of the dissipation of kinetic energy by Godunov methods. Firstly, as computational power and grid size increases, numerical simulations can resolve relatively low Mach number perturbations. An example of this is in the simulation of compressible turbulent flows. The large scales are at a relatively high Mach number, whereas small instabilities can occur at low Mach number. These can grow in size and affect the development of the larger scales (especially in fundamental instabilities such as Rayleigh Taylor, Richtmyer–Meshkov and Kelvin–Helmholtz). Critically, Godunov methods were largely designed for the simulation of flows with a steady frame of reference – typically those involving relatively smooth flow fields containing isolated discontinuities. Modern computing power allows simulations of flows, which are without a steady frame of reference in time and space, where velocities, pressure and density vary continuously throughout the flow field. It is important to understand the mechanism of dissipation of turbulent kinetic energy within high-resolution shock-capturing schemes, to better represent the growth of small instabilities, and hence reliably model the actual flow physics.

Secondly, a there has been a rapid increase in the use of implicit large eddy simulation in a variety of applications [10,11], where the dissipation inherent within the numerical method is employed 'in lieu' of an explicit subgrid model. To design future implicit models, an analytical description of the leading order dissipative terms is required so that this can be matched to the expected dissipation rate (such as that due to Kolmogorov's refined similarity hypothesis [12]).

The layout of the paper is as follows: Section 2 derives an equation to link entropy generation with dissipation of kinetic energy. By considering both entropy generation and kinetic energy dissipation together, it is easier to understand the mechanism of numerical dissipation. For example, it is expected that understanding of the kinetic energy dissipation rate should describe the increase in dissipation at low Mach numbers. Section 3 shows that the dissipation due to a shock of fixed strength is constant with Mach number at leading order, thus this cannot be the leading source of dissipation of kinetic energy (or generation of entropy). Next, the possibility that there are more shocks in the discrete Riemann problem at low Mach numbers is investigated in Section 4. It is shown that although the structure of the problem does change at low Mach number, this is not the direct source of increase of dissipation as it does not change significantly below a Mach number of

≈ 0.2. Section 5 demonstrates via an asymptotic analysis of the discrete problem that the leading order dissipation is due primarily to the reaveraging process and that the irreversible dissipation of kinetic energy is proportional to the magnitude of the velocity gradient squared multiplied by the speed of sound. This is validated numerically using several different Riemann solvers, exact and approximate. Finally, the analysis is extended to include higher order methods in space and time.

2. The relationship between kinetic energy and entropy

Before commencing the analysis, it is important to clarify the governing equations and essential to discuss the relationship between kinetic energy and entropy. This paper is concerned solely with the analysis of the Euler equations of gas flow, where the viscosity is assumed negligible ($Re \to \infty$). The homogeneity property of the Euler equations means that the properties can be analysed using the following governing equations in each principal direction:

$$\frac{\partial \mathbf{U}}{\partial t} + \frac{\partial \mathbf{E}}{\partial x} = 0, \tag{1}$$

where

$$\mathbf{U} = [\rho, \rho u, \rho v, \rho w, E]^{\mathrm{T}}, \tag{2}$$

$$\mathbf{E} = \left[\rho u, \rho u^2 + p, \rho uv, \rho uw, (E+p)u\right]^{\mathrm{T}}, \tag{3}$$

$$E = \rho e + 0.5\rho(u^2 + v^2 + w^2) \tag{4}$$

and ρ, e, u, v, w are the density, specific internal energy per unit volume and Cartesian velocity components, respectively. Throughout this paper it is assumed that the fluid satisfies the ideal gas equation of state

$$p = \rho e(\gamma - 1), \tag{5}$$

where γ is the ratio of specific heats. In a Godunov method the governing equations are solved in integral form where the cell averaged conserved variables at the new time step, $\overline{\mathbf{U}}^{n+1}$, are computed according to

$$\overline{\mathbf{U}}^{n+1} = \overline{\mathbf{U}}^{n} - \frac{\Delta t}{\Delta x}(\mathbf{E}_{i+1/2} - \mathbf{E}_{i-1/2}) = 0, \tag{6}$$

where Δt and Δx are the time step and width of the cell. The time averaged numerical fluxes $\mathbf{E}_{i\pm 1/2}$ are computed from the Riemann problem at the cell interface. This is typically seen as the solution of the Riemann problem along the line $x/t = 0$, where x is centred at the interface. At any interface where the velocity or pressure differs from one side to the next, the solution will normally split into three waves, a contact surface sandwiched by two waves which are either a shock or rarefaction. Only the shock wave adds irreversible dissipation, as the rarefaction and contact surface are isentropic phenomena. Thus, irreversible dissipation occurs only when the solution to the Riemann problem at $x/t = 0$ (the star quantities) lies between the contact surface and the shock wave.

Understanding the role of entropy in the context of dissipation of specific kinetic energy is key to understanding the dissipative properties of Godunov methods. Specific entropy is defined through the Gibbs equation (see for example [13] for a full derivation),

$$\mathrm{d}S = \frac{1}{T}\mathrm{d}e - \frac{p}{\rho^2 T}\mathrm{d}\rho, \tag{7}$$

where T is the temperature of the system. Integrating this equation gives

$$S = c_{\mathrm{v}} \ln\left(\frac{T^{n+1}}{T^n}\right) - R\ln\left(\frac{\rho^{n+1}}{\rho^n}\right) + S^n, \tag{8}$$

where S^n is the initial entropy at time n, c_{v} is the specific heat at constant volume and R is the specific gas constant. Noting that $T = p/(R\rho)$ and $c_{\mathrm{v}} = R/(\gamma - 1)$, the above equation can be rearranged into the following form for a change of entropy ΔS

$$\Delta S = \frac{R}{\gamma - 1} \ln \left[\left(\frac{p}{\rho^\gamma} \right)^{n+1} \left(\frac{\rho^\gamma}{p} \right)^n \right]. \tag{9}$$

The numerical solution to the Euler equations is constructed in a such a form that mass, momentum and total energy are conserved, but kinetic energy is not conserved due to numerical dissipation. The behaviour of the change of kinetic energy within a compressible fluid is similar to that of a damped spring. There are changes of kinetic energy, which are accompanied by an isentropic change in pressure, as is the case for an ideal inviscid flow without shocks. In this case, although the kinetic energy has changed, there has been no actual dissipation of kinetic energy and thus the flow behaves like an undamped spring. However, if the entropy increases then there has been an irreversible dissipation of specific kinetic energy, which acts as a dampener to the isentropic motion.

A direct relationship between kinetic energy and entropy will now be derived, assuming a continuous (infinitely differentiable) flow field. The derivation begins with the conservation equation for kinetic energy in vector notation without external forces,

$$\rho \frac{D}{Dt} \left(\frac{1}{2} V^2 \right) = -[\nabla \cdot (p\mathbf{u}) - p \nabla \cdot \mathbf{u}] + \mathcal{D}_\mathrm{w} - \mathcal{D}_\eta, \tag{10}$$

where ρ is the density, $V = \sqrt{u^2 + v^2 + w^2}$, p is the pressure, $\mathbf{u}$ is the vector of velocities, D/Dt represents the material or total derivative. The first group of terms on the right hand side relates to flow work due to the pressure on the control volume minus the work that does not increase the kinetic energy. By analogy to the Navier–Stokes equations (where $\mathcal{D}_\mathrm{w} = \nabla \cdot (\tau \cdot \mathbf{u})$, and $\mathcal{D}_\eta = \tau : \nabla \mathbf{u}$) $\mathcal{D}_\mathrm{w}$ is the total work that the surroundings do on the fluid through the numerical shear stress and $\mathcal{D}_\eta$ is the portion of the work due to numerical shear stresses, which dissipates kinetic energy. For some numerical methods the analogy with the Navier Stokes equations can be considered directly, for example, it was shown by Fureby and Grinstein [14] that the numerical viscosity of FV methods can be written as a shear stress τ. Note that in this derivation it is assumed that positive numerical viscosity exists, however the form of the numerical viscosity does not need to be specified. Conservation of total energy without external forces for the fluid under consideration gives,

$$\rho \frac{D}{Dt} \left(e + \frac{1}{2} V^2 \right) = -\nabla \cdot \mathbf{q} - [\nabla \cdot (p\mathbf{u}) - p \nabla \cdot \mathbf{u}] + \mathcal{D}_\mathrm{w}, \tag{11}$$

where $\mathbf{q}$ is the numerical heat diffusion. By subtracting the kinetic energy equation from the total energy equation, a conservation equation for internal energy e without external sources can be written

$$\rho \frac{D}{Dt} (e) = -\nabla \cdot \mathbf{q} - p \nabla \cdot \mathbf{u} + \mathcal{D}_\eta. \tag{12}$$

Note that the sink term due to numerical dissipation present in the kinetic energy equations appears identically in the internal energy equation as a source term. There is an additional source term due to the numerical heat diffusion flux $\mathbf{q}$ and due to pressure work compressing the element.

Entropy is a scalar quantity which is transported with the heat flow rate $\mathbf{q}$. The transport equation for entropy is [13]

$$\rho \frac{Ds}{Dt} = -\nabla \cdot \left(\frac{\mathbf{q}}{T} \right) + \dot{\mathcal{P}}_\mathrm{s}, \tag{13}$$

where the first term on the right hand side represents flux of entropy via heat conduction, $\dot{\mathcal{P}}_\mathrm{s}$ is the production rate of entropy and T is the temperature. Next, using the Gibbs equation

$$\rho \frac{Ds}{Dt} = \frac{\rho}{T} \frac{De}{Dt} - \frac{p}{\rho T} \frac{D\rho}{Dt}. \tag{14}$$

Combining this with the continuity equation and equation for the evolution of internal energy gives [15]

$$\dot{\mathcal{P}}_\mathrm{s} = \frac{\mathbf{q} \nabla T}{T^2} + \frac{\mathcal{D}_\eta}{T}. \tag{15}$$

The second term on the right hand side refers to a production of entropy via shear stresses and is identical to the sink term in the kinetic energy equation divided by temperature. Consider a typical low Mach number flow, where it is assumed that production of entropy due to numerical thermal conduction is small in comparison to production via numerical shear stresses. For this case, temperature multiplied by production of entropy is equal to the irreversible numerical shear dissipation in Eq. (10), or

$$T\dot{\mathcal{P}}_s = \mathcal{D}_\eta = -\frac{1}{2}\rho\left(\frac{D(V^2)}{Dt}\right)_{\text{irreversible}}. \tag{16}$$

The result directly relates the increase of entropy with the dissipation of kinetic energy pointwise within a system due to the presence of numerical dissipation of kinetic energy $\mathcal{D}_\eta$. No assumption has been made of the form of the dissipation of kinetic energy, hence this analysis is valid for both physical and numerical dissipation.

A useful property of the directional split Godunov methods is that many of the properties of the scheme can be illustrated through simple one-dimensional test cases, such as the combination of isentropic and non-isentropic behaviour. Consider the shock tube problem

$$x < 0.5, \quad p_L = p_R = p_0\left(1 + \frac{\gamma-1}{2}M^2\right)^{\frac{\gamma}{(\gamma-1)}}, \quad u = Ma/2, \tag{17}$$

$$x > 0.5, \quad \rho_L = \rho_R = \rho_0\left(1 + \frac{\gamma-1}{2}M^2\right)^{\frac{1}{(\gamma-1)}}, \quad u = -Ma/2, \tag{18}$$

where a is the speed of sound and M is the Mach number. The computational domain is 200 cells in a region of dimension 1 and the boundary conditions are periodic. First-order time-stepping and first-order piecewise constant in space reconstruction is used. This problem is formulated so that the left and right hand quantities are isentropic realisations of the same flow and that the mean momentum is zero. Fig. 1a shows the variation of specific kinetic energy with time compared to the variation of $T\Delta S$ where the values of p_0 and ρ_0 are chosen such that the Mach number of the flow is 0.1. The kinetic energy behaves as a damped spring as described previously, where the isentropic variations in kinetic energy are much more rapid than the non-isentropic variations. However, it is clear that the irreversible decrease in kinetic energy is mirrored exactly by an increase in $T\Delta S$. Fig. 1b shows the same test case for a Mach number of 0.01. The same relationship can be seen, however the rate of decrease of kinetic energy is much more rapid, illustrating the strong Mach number dependence of dissipation of kinetic energy.

As a more complex case, consider homogeneous decaying turbulence in a periodic cube at resolution 32^3 using the fifth-order MUSCL reconstruction in space and the third-order TVD Runge–Kutta in time. Following [16,11], the initial condition is specified as a summation of Fourier modes of random phase corresponding to the kinetic energy spectra

$$E(k) = u^2\frac{k^4}{k_p^4}\sqrt{\frac{8}{k_p^2\pi}}\exp(-2(k/k_p)^2), \tag{19}$$

where k is the wave number and the peak of the energy spectrum was chosen at $k_p = 4$. Additionally, the initial kinetic energy magnitude and Mach number are chosen as

$$\text{KE} = \frac{3}{2}u^2 = 0.5, \tag{20}$$

$$M = \frac{u}{c} = 0.1, \tag{21}$$

where u is the mean turbulent velocity. Fig. 2 shows the time variation of kinetic energy compared to the initial kinetic energy minus $T\Delta S$. The agreement is exact. From these two examples it is clear that if the behaviour of entropy is understood, then an understanding of the dissipation of kinetic energy by Godunov schemes follows naturally.

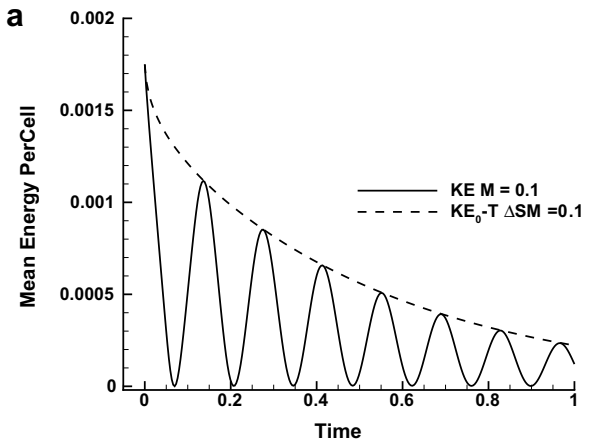

$M = 0.1$

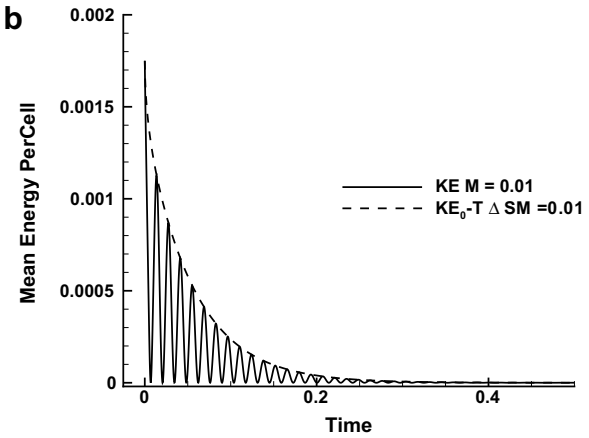

$M = 0.01$

Fig. 1. Actual change of kinetic energy plotted with the predicted change using the initial kinetic energy minus $T\Delta S$ for a shock tube problem.

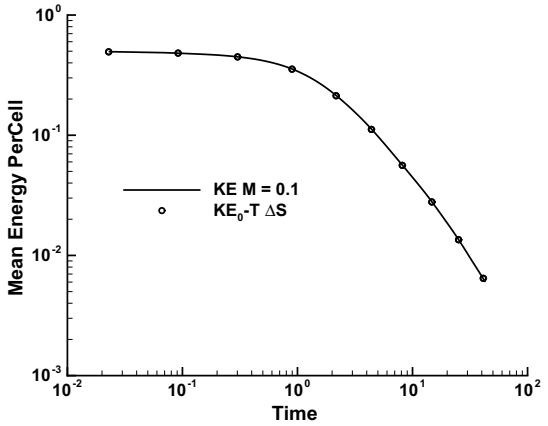

Fig. 2. Actual change of kinetic energy plotted with the predicted change using the initial kinetic energy minus $T\Delta S$ for homogeneous decaying turbulence in a cube.

3. The dissipation of kinetic energy across a shock wave

The passage of a shock wave causes an increase in entropy, thus leads to irreversible dissipation of kinetic energy. Consider a stationary shock wave with preshock velocity u, specific volume $\mathcal{V}$, Temperature T and pressure p. Bethe [17] (reproduced in [18]) utilised the Hugoniot relations to derive the leading order entropy increase as

$$\Delta S = -\left.\frac{\partial^2 p}{\partial \mathcal{V}^2}\right|_S \frac{\Delta \mathcal{V}^3}{12T}. \tag{22}$$

This relationship is accurate to within 15% where $\Delta u/u$ and $\Delta\rho/\rho$ are less than 10% and $M_s < 1.05$. From thermodynamic principles the second derivative of the pressure with respect to the specific volume can be expressed as [19]

$$\left.\frac{\partial^2 p}{\partial \mathcal{V}^2}\right|_S = \frac{2\mathcal{G}\gamma p}{\mathcal{V}^2}, \tag{23}$$

where $\mathcal{G}$ is the curvature of the isentrope. Using Eq. (23) in (22) gives

$$\Delta S = -\frac{\mathcal{G}a^2}{6T}\left(\frac{\Delta \mathcal{V}}{\mathcal{V}}\right)^3. \tag{24}$$

Considering conservation of mass across a stationary shock

$$\frac{u_1}{\mathcal{V}} = \frac{u_2}{\mathcal{V}_2}, \tag{25}$$

where u_1 and u_2 are the pre- and post-shock flow velocities, $\mathcal{V}$ and $\mathcal{V}_2$ the pre- and post-shock specific volumes, the difference in specific volume $\Delta\mathcal{V}$ can be related to the difference in velocity

$$\frac{\Delta \mathcal{V}}{\mathcal{V}} = \frac{\Delta u_s}{u_1}, \tag{26}$$

where Δu_s is the velocity jump at the shock. The change of entropy can now be written as

$$\Delta S = -\frac{\mathcal{G}a^2}{6T}\left(\frac{\Delta u_s}{u_1}\right)^3. \tag{27}$$

Finally, as noted in [19] the curvature of the isotrope for an ideal gas is

$$\mathcal{G} = \frac{1}{2}(\gamma + 1). \tag{28}$$

Inserting this into Eq. (27), the irreversible increase of specific internal energy $T\Delta S$ is

$$T\Delta S = -\frac{(\gamma+1)a^2}{12}\left(\frac{\Delta u_s}{u_1}\right)^3. \tag{29}$$

As this is relative to a stationary shock, then as the Mach number tends to zero, $u_1 \to a$, showing that the dissipation of a shock of fixed Mach number decreases proportionally to $1/a$. However, the shock wave travels at a speed proportional to a thus the *dissipation rate* due to the passage of a shock of fixed Mach number is constant in time and independent of flow Mach number. This demonstrates that the increase in dissipation at low Mach numbers is not physical, but is a property of the discrete system.

4. The form of the solution to the discrete Riemann problem

As the dissipation due to a shock wave is not dependent on the flow Mach number, then the sources of generation of entropy in the discrete system must be identified and examined. The sources are most easily classified by considering the 'reconstruct-solve-average' picture of Godunov methods as suggested by Leveque [20]. In the discrete system, entropy generation will occur in all three stages. Entropy generation in the

reconstruction stage will be dealt with in Section 5.3, as at present the focus is on first-order piecewise constant reconstruction. This section examines the increase of entropy in the 'solve' part of the process, due to changes in the solution to the Riemann problem computed at the cell interface at low Mach number. It is possible that the number of interfaces where the solution of the Riemann problem lies between the shock and contact surface increases as the Mach number decreases, thus causing an increase in the rate of generation of entropy.

To compute the solution to the Riemann problem exactly an iterative process must be employed to determine the velocity v^*, density ρ^* and pressure p^* between the waves. However, at low Mach number or where the jumps are not extreme, the solution to the Riemann problem can be attained with reasonable accuracy using the primitive variable linearised solution [21] for p^*

$$p^* = \frac{1}{2}(p_L + p_R) + \frac{1}{2}(u_L - u_R)\bar{\rho}\bar{a}, \tag{30}$$

which can be rearranged as

$$p^* = p_R + \underbrace{\frac{\Delta p}{2}}_{\mathcal{O}(M^2)} + \underbrace{\frac{\Delta u}{2}\bar{\rho}\bar{a}}_{\mathcal{O}(M)}. \tag{31}$$

Scaling arguments can be used to deduce the behaviour of the flow field at low Mach number. It is commonly accepted that, in the absence of acoustic waves, pressure differences in an incompressible flow field scale with M^2, and velocity differences scale with M (see for example [1,2,22,23]). The second term on the left hand side of Eq. (31) is $\mathcal{O}(M^2)$ whereas the final term scales as $\mathcal{O}(M)$. This means that in low Mach number flows it is expected that the majority of Riemann problems will result in a two-shock or two-rarefaction configuration, as pointed out in [9]. These are generated when $p^* < \max(p_L, p_R)$ or $p^* < \min(p_L, p_R)$, respectively.

Indeed, examining each cell interface for the homogeneous decaying turbulence problem shows that at Mach number 0.2 the structure of the field is 46% two-shock, 46% two-rarefaction and 7% single-shock, single-rarefaction solutions. Reducing the Mach number to 0.02 gives 48% two-rarefaction and 52% two-shock. This does not change as Mach number decreases. As expected, as the Mach number decreases the occurrence of single-shock, single rarefaction solutions becomes increasingly rare. The typical structure of the solution to the Riemann problem changes as the Mach number decreases, however, once $M < 0.1$ the structure does not change significantly and so is not likely to be the direct cause of increased dissipation.

5. Irreversible dissipation due to solution reaveraging

5.1. Linear advection equation

The linear advection equation is particularly useful to demonstrate the irreversible dissipation of kinetic energy in the FV framework. Consider

$$u_t + a u_x = 0, \tag{32}$$

where u can be taken as a velocity and a is the signal speed, assumed positive. In this case there are no dissipative terms thus the exact solution conserves kinetic energy. The problem can be discretised at first-order accuracy in time and upwind in space as follows:

$$u_i^{n+1} = u_i^n - va(u_i^n - u_{i-1}^n), \tag{33}$$

where $v = \Delta t/\Delta x$. Taking the initial conditions as $u_{i-1}^n = -\Delta u/2$ and $u_i^n = u_{i+1}^n = \Delta u/2$, consider the solution in cell i at time $n+1$

$$u_i^{n+1} = \frac{\Delta u}{2}(1 - 2va). \tag{34}$$

The theoretical change in kinetic energy is zero, but computationally it is

$$(u_i^{n+1})^2_{\text{exact}} - (u_i^{n+1})^2_{\text{numerical}} = \frac{1}{2}\Delta u^2 va(1 - va), \tag{35}$$

giving a dissipation rate increasing proportional to Δu^2 and the speed of sound a. Note that this result can also be gained via standard modified equation analysis [21]. It was also shown by Merriam [24] that the production of entropy (defined by the entropy pair $S = -u^2$ and $F = -cu^2$) for the wave equation in this first-order scheme is proportional to Δu^2 and a, mirroring the decrease in kinetic energy shown here. As the flux is exact, the dissipation is due solely to the reaveraging process where $\overline{u}^2 \neq \overline{(\overline{u} + u')^2}$. This implies that a similar dissipation due to the reaveraging process should occur in the FV representation of the Euler equations. The following section investigates this by examining the variation of the entropy over a single time step.

5.2. The Euler equations

To derive the actual change of entropy in the discrete system, the entropy change in a single computational cell in a single time step is considered. The derivation of the leading order entropy change for the case of an isolated jump in velocity is detailed in full in Appendix A to allow the reader to repeat the analysis. This solution was first gained by hand and was subsequently used to validate solutions gained using the symbolic manipulation software Mathematica for the more complex but common case of a jump in all primitive variables.

5.2.1. Isolated velocity discontinuity

In this section the change of entropy is derived for an interface where there is a velocity jump Δu, but ρ and p remain constant. Consider flow through three computational cells, where the discontinuity is located at $i + 1/2$ as shown in Fig. 3. The flow variables are evolved over one time step for a first-order in space and time upwind Godunov scheme. It is assumed that the solution of the Riemann problem can be approximated using the linearised solution [21, p. 279], an assumption which is validated in subsequent numerical test cases. Assuming quantities ρ, Δu and p in the cell $i - 1$ and i, and ρ, 0 and p in cell $i + 1$ at time level n, the solution of the Riemann problem at the cell interface $i + 1/2$ can be written as

$$p^* = p + \frac{\Delta u \rho a}{2}, \tag{36}$$

$$u^* = \frac{\Delta u}{2}, \tag{37}$$

$$\rho^* = \rho + \frac{\Delta u \rho}{2a}. \tag{38}$$

The leading order entropy increase over a single time step given by an asymptotic expansion in Δu and a is (see Appendix A for full details)

$$\Delta S = \frac{R\gamma v \Delta u^2}{4a}(1 - va) + \mathcal{O}(\Delta u^3). \tag{39}$$

As the irreversible increase of specific internal energy is $T\Delta S = (a^2/R\gamma)\Delta S$ then

$$T\Delta S = \frac{\Delta u^2 va}{4}(1 - va) + \mathcal{O}(\Delta u^3). \tag{40}$$

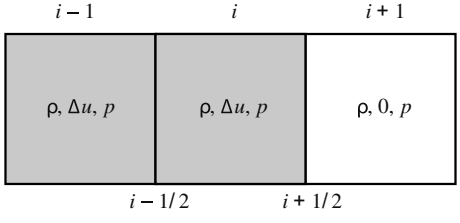

Fig. 3. Schematic of the flow under consideration.

Table 1
Rate of increase of $T\Delta S$ for an isolated velocity jump per unit time

$\Delta u/a$	Eq. (41)	Exact	PVRS	HLLC
0.5	0.00024	0.00026	0.00025	0.00026
0.1	0.0011	0.0011	0.0011	0.0011
0.01	0.01	0.01	0.01	0.01
0.001	0.104	0.104	0.104	0.104

It can be seen that the increase of entropy is only positive as long as $1 - va > 0$, which is the low Mach number limit of the familiar CFL condition. Eq. (40) can be converted to time rate of dissipation, given that $v = \Delta t/\Delta x \approx \mathcal{C}/a$, where $\mathcal{C}$ is the Courant–Friedrichs–Lewy number,

$$\epsilon_{\Delta u} = T\Delta S/\Delta t = \frac{\Delta u^2 a}{4\Delta x}(1 - va) + \mathcal{O}(\Delta u^3), \tag{41}$$

where ϵ is the irreversible change of kinetic energy per unit time. This is consistent with analysis of the increase of entropy by Barth [25], which also points to an increase of entropy proportional to the jump size squared. Additionally, the entropy generation over the single time step is proportional to $1/a$, as opposed to $1/a^2$ predicted for the entropy rise over a shock wave (Eq. (29)).

The asymptotic analysis has been validated using a one-dimensional test case for a first-order in time and space Godunov method solving the Riemann problem with an exact Riemann solver, the HLLC solver and the primitive variable Riemann solver (for details about these Riemann solvers consult [21]). Table 1 shows the rate of entropy increase in the first time step for a shock tube case where the left and right states are defined as

$$p_L = p_R = \rho a^2, \quad \rho_L = \rho_R = \rho, \quad u_L = \Delta u, \quad u_R = 0. \tag{42}$$

The results show excellent agreement with all numerical schemes even where the Mach number of the velocity jump is as high as 0.5. This agreement is to be expected as Eq. (41) is a leading order approximation in terms of Mach number of the velocity jump and in terms of order of the velocity jump itself, thus it is applicable beyond the incompressible regime.

The dependence of the dissipation rate on the speed of sound and Δu^2 is clearly different from the dissipation inherent in the solution of the Euler equations (Eq. (29)). Eq. (29) was derived assuming the validity of the Hugoniot relations [26], which only hold true when all gradients of the flow exiting the control volume are zero, and the rate of change of these gradients is zero in a given frame of reference. Clearly, this is not the general case for an arbitrary interface where there is a difference in all primitive variables. Thus, the Hugoniot relations hold in a global sense, but the above expansion applies in the case of unsteady flow for an interface with a local variation in velocity from the left to right state.

Taking the initialisation of a shock wave on a grid as an example, the validity of the result becomes clear. In the first time step a dissipation proportional to Δu_s^2 acts on the initialised velocity jump. This is larger than the dissipation rate for an ideal shock wave derived by Bethe and thus the shock is diffused. After several time steps a steady state solution is gained where the sum of several smaller Δu^2 equals the entropy gain of a single global increase proportional to Δu^3. In this process the excess entropy produced in the first time step at a rate of Δu_s^2 manifests itself as an entropy 'anomaly'. It has also been termed 'wall heating', although this is slightly misleading as the entropy errors occur throughout the flow field. A similar process occurs when shock waves interact and causes excess heating in the Noh test case, which can be viewed as a shock interaction problem [3].

The dependence on Δu^2 is due to an interaction of both the governing equations and the reaveraging process. If the increase of entropy was solely due to the reaveraging of the continuous function to a fixed mesh, then the leading order error terms would be of order Δu. However, the governing equations are constructed in such a manner that the leading order fluctuations (i.e. Δp and $\Delta\rho$) are isentropic in nature and so cancel in the asymptotic expansion.

Menikoff [7] examined the variation of entropy when initialising a shock wave, or when shock waves interact and demonstrated that an entropy anomaly occurs due to the finite width of a viscous shock profile, which is a special case of the general asymptotic expansion presented here.

As also observed numerically in [7], under refinement of the mesh the spatial extent of the anomaly reduces, but the magnitude does not. Thus, in employing a Godunov method to simulation a turbulent flow field, there is no steady frame of reference and these entropy 'anomalies' occur throughout the field providing a dissipation rate proportional to Δu^2 and a. It is then expected that ILES simulations using a Godunov method would have a subgrid model more akin to a physical viscosity than proportional to Δu^3 as ideally desired. As the numerical viscosity increases above that required to mimic the behaviour of the subgrid scales then a greater separation is required between the highest wave number captured on the grid and the beginning of the subinertial range. When simulating low Mach number turbulence with Godunov methods this effect means that a large number of finite volumes must be employed to give the required separation. This explains why the kinetic energy spectra gained using shock-capturing Godunov-type methods are typically overly dissipative in the high wave number range (see for example [27,28]).

5.2.2. Isolated velocity and pressure discontinuity

The analytical methodology followed in Appendix A to give the leading order dissipation rate for an isolated velocity discontinuity has been implemented into Mathematica, a symbolic manipulation software package. The use of symbolic manipulation software enabled the derivation of leading order dissipation rates for more complex cases including jumps in all primitive variables. This was validated using the analytical solution for the isolated velocity jump and numerical test cases. The Mathematica script used to compute the leading order terms in the dissipation rate for the case of a jump in all primitive variables is reproduced in Appendix B.

Extending the previous test case but now including a jump in pressure, such that

$$p_{\mathrm{L}} = p + \Delta p/2, \quad p_{\mathrm{R}} = p - \Delta p/2, \quad \rho_{\mathrm{L}} = \rho_{\mathrm{R}} = \rho, \quad u_{\mathrm{L}} = \Delta u, \quad u_{\mathrm{R}} = 0, \tag{43}$$

the leading order dissipation rate in the presence of a jump Δp and Δu, $\epsilon_{\Delta p,\Delta u}$, can be written as

$$\epsilon_{\Delta u,\Delta p} = \frac{(1 - va)}{\Delta x} \frac{(\Delta p - \rho a \Delta u)^2}{4a\rho^2} + \cdots \tag{44}$$

The time rate of irreversible dissipation of specific kinetic energy in the case of an isolated pressure jump decreases with Mach number (assuming a fixed pressure jump). Table 2 details the rate of entropy increase in the first time step for a first-order in time and space shock tube test case where the initial conditions are

$$p_{\mathrm{L}} = p + \Delta p/2, \quad p_{\mathrm{R}} = p - \Delta p/2, \quad \rho_{\mathrm{L}} = \rho_{\mathrm{R}} = \rho, \quad u_{\mathrm{L}} = u_{\mathrm{R}} = 0 \tag{45}$$

and Δp is constant in magnitude, the ratio $\Delta p/p$ is adjusted by increasing the pressure p. The highest change tested is a jump of half the magnitude of the mean pressure of the left and right side. In all cases the error between the leading order entropy increase in Eq. (44) and the exact solution is less than 1%. The rate of entropy production scales with the inverse of the speed of sound as expected. Comparing this with the results in Table 1 it is clear that the terms due to the velocity jump dominate in low Mach number flows. Interestingly, the leading order approximation in Eq. (44) is valid for such a large pressure jump even though the PVRS Riemann solver produces negative entropy due to the higher order terms.

In this case, the variations in density do not affect the rate of entropy production – it only modifies the magnitude of production in the presence of a velocity or pressure jump due to the influence of the term $\rho = (\rho_{\mathrm{L}} + \rho_{\mathrm{R}})/2$ in the linearised solution.

It is interesting to note that the dissipation is proportional to the square of the departure from the characteristic relation along the $\lambda = u + a$ eigenvalue, $\Delta p - \rho a \Delta u = 0$. In an ideal incompressible flow the quantity

Table 2
Rate of increase of $T\Delta S$ for an isolated pressure jump per unit time

$\Delta p/p$	Eq. (44)	Exact	PVRS	HLLC
0.5	0.00048	0.00048	-0.0001	0.00048
0.1	0.00021	0.00021	0.00016	0.00021
0.01	6.6×10^{-5}	6.6×10^{-5}	6.5×10^{-5}	6.6×10^{-5}
0.001	2.1×10^{-5}	2.1×10^{-5}	2.1×10^{-5}	2.1×10^{-5}

$\rho a \Delta u$ is of order M, compared to pressure which is of order M^2, meaning that this is not likely to become small at low Mach number.

The analysis within this subsection has assumed that u^* is positive, i.e. that the solution at $x/t = 0$ lies to the left of the contact surface and thus can be described by Eq. (38), but there is no assumption in the direction of the jumps as long as this criterion remains valid. If it is assumed that the velocity jump is sufficiently negative, or that the pressure increases from left to right such that $u^* < 0$ then the solution for ρ^* changes to [21, p. 297]

$$\rho^* = \rho_R + (u^* - u_R)\rho/a. \tag{46}$$

Utilising the script in Appendix B, the leading order rate of dissipation in this case is

$$\epsilon_{u^*<0} = \epsilon_{\Delta u,\Delta p} + \frac{\Delta p(\Delta p - a^2\Delta\rho)}{2\Delta x \rho^2 a(\gamma - 1)} + \cdots \tag{47}$$

For a constant pressure and density jump there is an additional component of dissipation which increases as the Mach number decreases, proportional to $\Delta p \Delta\rho$. However, this would scale as M^{-4} in incompressible flows or at least M^{-2} for unpreconditioned compressible FV schemes so would not dominate over the terms in Δu^2. The characteristic invariant along the $\lambda = u$ eigenvalue also appears in this expression, so it appears that dissipation is minimised only when all jumps are zero, or when the jumps correspond exactly to the characteristic equations for the waves passing into the cell.

5.2.3. Shear waves

For a three-dimensional direction split method the shear waves are typically advected passively. This means that the accuracy of the projected value of the velocities parallel to the interface, in this case the v velocity, will also affect dissipation. In the case of a single isolated jump in v velocity it is expected that dissipation will only occur if the contact wave enters the cell under consideration. This is because the components parallel to the interface only change across the contact surface. For example, if the jump in v velocity takes place at the right hand interface, dissipation occurs only if u^* is negative.

Following the methodology detailed in Appendix A, the leading order irreversible dissipation rate has been derived given the initial conditions in Eq. (43) and additionally $v_L = \Delta v/2$, $v_R = -\Delta v/2$. The leading order term is constant with respect to the speed of sound,

$$\epsilon_{\Delta v} = \frac{\Delta v^2(\Delta\rho - 2\rho)u}{4\rho\Delta x} + \cdots, \tag{48}$$

thus it does not influence the asymptotic behaviour of the system. In a simple shock tube case with constant u, p, ρ and a step discontinuity in the v velocity component Eq. (48) is accurate to within 1% in validation cases where $\Delta v/a < 0.5$.

5.3. Higher order methods

5.3.1. Temporal discretisation

The analysis within the previous subsections is not valid for higher order time-stepping methods and would have to be repeated for each different time-stepping method. As all higher order methods are multi-step then it is expected that the resulting expressions would be quite complex. However, the asymptotic behaviour can easily be examined numerically. Table 3 shows the velocity jump test case in Section 5.2 repeated using second-

Table 3
Rate of increase of $T\Delta S$ for a fixed magnitude velocity jump (varying the speed of sound) for several different time stepping methods

$\Delta u/a$	2nd TVD RK	2nd DT	3rd TVD RK	3rd ES RK
0.5	0.00028	0.00023	0.00029	0.0003
0.1	0.0012	0.0010	0.0012	0.0014
0.01	0.011	0.010	0.013	0.013
0.001	0.118	0.103	0.130	0.130

order total variation diminishing (TVD) Runge–Kutta method [29], implicit–explicit dual time-stepping (DT) method [30], third-order TVD Runge–Kutta method [31] and third-order extended stability (ES) Runge–Kutta [32] with first-order spatial reconstruction using the exact Riemann solver. These results demonstrate that the dissipation increases linearly with speed of sound with all time stepping methods as was the case for the first-order in time computations. Additional tests varying the magnitude of isolated velocity discontinuities whilst holding the speed of sound constant are detailed in Table 4. It confirms that the dissipation rate is proportional to Δu^2 for all higher order time-stepping methods examined. This confirms that the same trends detailed for the first-order schemes apply to higher order in time computations.

5.3.2. Spatial discretisation

The previous sections discuss only the first-order in space Godunov method. The majority of practical simulations are conducted with second or even higher order methods in space and so it is useful to extend the above analysis. This subsection analyses the dissipative properties of a Godunov method employing a second-order accurate MUSCL reconstruction with the van Leer limiter [33]. The left and right interface variables are defined from

$$\mathbf{P}^{\mathrm{L}}_{i+1/2} = \mathbf{P}_i + \frac{1}{2}\boldsymbol{\phi}^{\mathrm{lim}}(\mathbf{r}^{\mathrm{lim,L}})(\mathbf{P}_i - \mathbf{P}_{i-1}), \tag{49}$$

$$\mathbf{P}^{\mathrm{R}}_{i+1/2} = \mathbf{P}_{i+1} - \frac{1}{2}\boldsymbol{\phi}^{\mathrm{lim}}(\mathbf{r}^{\mathrm{lim,R}})(\mathbf{P}_{i+2} - \mathbf{P}_{i+1}), \tag{50}$$

where $\mathbf{P}$ is the vector of cell averaged primitive variables and the cells are labelled by the integer i. Also,

$$\mathbf{r}^{\mathrm{lim,L}}_i = \frac{\mathbf{P}_{i+1} - \mathbf{P}_i}{\mathbf{P}_i - \mathbf{P}_{i-1}}, \quad \mathbf{r}^{\mathrm{lim,R}}_i = \frac{\mathbf{P}_i - \mathbf{P}_{i-1}}{\mathbf{P}_{i+1} - \mathbf{P}_i}. \tag{51}$$

The van Leer limiter can be written as

$$\boldsymbol{\phi}^{\mathrm{lim}}_{VL} = \frac{2\mathbf{r}^{\mathrm{lim}}}{1 + \mathbf{r}^{\mathrm{lim}}}. \tag{52}$$

Additionally, it is constrained to first-order at maxima and minima in the standard manner. There are two key differences when employing variable extrapolation methods; firstly they increase the cell averaged kinetic energy within a given cell via the process of interpolation itself (relative to piecewise constant methods) and change the total entropy within the cell; secondly, in smooth regions, higher order interpolation in space would act to reduce the magnitude of the jumps between the left and right quantities.

Following standard modified equation analysis [34,35] it can be shown that a Taylor series expansion of MUSCL reconstruction using the van Leer interpolation method of the vector of cell averaged primitive variables $\mathbf{P}$ gives

$$\tilde{\mathbf{P}}^{\mathrm{R}}(x) = \mathbf{P}^i + \frac{\Delta x}{2}\mathbf{P}^i_x + \Delta x^3\left(-\frac{(\mathbf{P}^i_{xx})^2}{8\mathbf{P}^i_x} + \frac{1}{12}\mathbf{P}^i_{xxx}\right) + \mathcal{O}(\Delta x^5), \tag{53}$$

where $\mathbf{P}^i$ indicates functions evaluated at the cell centre. The exact expansion from the cell averaged quantity to the continuous function gives

$$\mathbf{P}(x) = \mathbf{P}^i + \frac{\Delta x}{2}\mathbf{P}^i_x + \frac{\Delta x^2}{12}\mathbf{P}^i_{xx} + \mathcal{O}(\Delta x^4), \tag{54}$$

Table 4
Rate of increase of $T\Delta S$ for a variable velocity jump (fixed speed of sound) for several different time-stepping methods

$\Delta u/a$	2nd TVD RK	2nd DT	3rd TVD RK	3rd ES RK
0.1	0.0012	0.0010	0.0012	0.0014
0.2	0.0052	0.0043	0.0055	0.0056
0.4	0.023	0.019	0.023	0.023

confirming that the van Leer limiter is second-order accurate in the MUSCL reconstruction. From this point on the superscripts $(.)^i$ will be omitted for clarity.

The generation of entropy during the solution of the Riemann problem and the subsequent time evolution of the cell average quantities can now be computed using the extrapolated variables. The process followed in Section 5.2.1 was repeated to compute the entropy rise, however with the key difference that the velocity is assumed to vary continuously through the group of three cells instead of employing a discontinuous initial condition. For discontinuous flows (e.g. a square wave initial condition) the traditional MUSCL and WENO schemes will reduce to the first-order solution in the first time step, as the construction of MUSCL schemes ensure piecewise constant reconstruction and the class of Essentially Non-Oscillatory methods will give extremely small weightings to the stencils which cross the discontinuity. Hence, the entropy increase in discontinuous flows will be identical to that predicted for the first-order scheme.

The fluxes at the $i+1/2$ and $i-1/2$ interfaces are computed from the Taylor series expansion of the van Leer extrapolation. These are then evolved at first-order in time and the change of entropy over the time step computed. The Mathematica script used to generate these results is included in Appendix C. Next, this process was repeated using the exact solution at the cell interfaces (i.e. the same process but with the exact Taylor series expansion). The leading order change in entropy in the discrete solution with van Leer limiting is then subtracted from the exact solution, giving the dissipation rate due to the errors in the spatial discretisation as

$$\epsilon_{\Delta u}^{\mathrm{VL}} = \frac{\Delta x^2}{12} u u_x u_{xx} + \frac{\Delta x^3 a}{24}(3u_{xx}^2 + (2\mathcal{C}-3)u_x u_{xxx}). \tag{55}$$

The second-order term is locally dispersive, however the third-order term is dissipative as long as the CFL constraint is satisfied. Furthermore, the dissipation rate is proportional to the magnitude of the velocity derivatives squared multiplied by the speed of sound. The leading order term is Δx^3 as expected, which is the leading order difference between the left and right van Leer interpolated quantities. This is consistent with the results of the first-order analysis.

The conclusions of this analysis have been tested numerically by examining the increase of entropy in the first time step from the following initial condition:

$$p_{\mathrm{L}} = p_{\mathrm{R}} = p_0/M^2, \quad \rho = \rho_0, \quad u = Ma\sin(4\pi x)/2, \tag{56}$$

where a is the speed of sound and M is the Mach number. The computational domain is 200 cells in a region of dimension 1, the boundary conditions are periodic and $\mathcal{C} = 0.5$. The object of this initial condition was to create a smooth flow field, as the dissipation rate for a discontinuous flow field could be heavily influenced by the first-order points. The test case uses third-order extended stability Runge–Kutta time-stepping with a second-order van Leer spatial discretisation and uses the exact Riemann solver.

Table 5 details the dissipation rate in the first time step as a function of Mach number. These results confirm that the dissipation rate increases inversely proportional to the Mach number as expected. Next, the pressure and density are fixed and the magnitude of the initial velocity is varied. This is to investigate the u^2 dependence of the dissipation rate. The results are detailed in Table 6, where it can be clearly seen that the dissipation rate is proportional to the velocity magnitude squared, again in excellent agreement with the theoretical result.

Finally, it is predicted that the entropy increase is proportional to Δx^3. Table 7 shows $T\Delta S$ for the same initial condition fixed at Mach number of 0.1 for three different grid sizes. Clearly, the dissipation rate is approximately proportional to Δx^3, as each doubling in grid points should decrease the dissipation eight-fold. There is a slight deviation at high resolution, which is due to the first-order points at the maxima and minima of the sine wave.

Table 5
Kinetic energy decay rate ϵ for a fixed magnitude velocity field (varying the speed of sound) using the second-order van Leer limiter with third-order ES RK over a single time step

M	ϵ	Normalised
0.1	3.00×10^{-5}	1
0.01	3.00×10^{-4}	10
0.001	2.97×10^{-3}	99

Table 6
Kinetic energy decay rate ϵ with increasing velocity magnitude (fixed speed of sound) using the second-order van Leer limiter with third-order ES RK over a single time step

M	ϵ	Normalised
0.1	3.00×10^{-5}	1
0.2	1.19×10^{-4}	4
0.4	4.84×10^{-4}	16

Table 7
Variation of entropy rise with grid size at Mach number 0.1 using the second-order van Leer limiter with third-order ES RK over a single time step

Grid points	$T\Delta S$	ϵ	Normalised
100	5.0×10^{-7}	2.4×10^{-4}	1
200	3.1×10^{-8}	3.0×10^{-5}	8
400	2.0×10^{-9}	4.0×10^{-6}	61

This confirms that the key parameter in the design of numerical schemes is to minimise the difference between the left and right quantities, not necessarily the formal order of accuracy. As an example of this, the Minmod and van Leer limiters have the same formal order of accuracy when used in a MUSCL formulation. Despite this the van Leer limiter will normally resolve interfaces much more sharply. The underlying reason for this difference is that although both limiters have second-order accurate interpolation, the jump from the left to right side interpolated values is second-order for Minmod, but third-order for van Leer. This gives the observed improvement in performance.

6. Conclusions

The analytical results derived within this paper demonstrate that the numerical dissipation rate of Godunov methods for a typical unsteady flow is not of the same form as the irreversible dissipation in the governing Euler equations. In shock tube cases the global dissipation of the solution for a shock wave can be computed using the Hugoniot relations and has been shown previously to be proportional to the velocity jump across the shock wave cubed. However, in the case of an unsteady flow feature, the local increase in entropy is dependent on the numerical viscosity which in the FV Godunov method is proportional to the magnitude of the velocity gradients squared over the speed of sound, a. Under the assumption of low production of entropy due to thermal gradients, this corresponds to a kinetic energy dissipation rate proportional to the speed of sound and magnitude of the velocity derivatives squared, explaining directly the poor performance of Godunov methods at low Mach numbers. The conclusions of the theoretical analysis have been numerically validated for first-order in time and space and second-order van Leer reconstruction in space with third-order Runge–Kutta time integration. The analysis has shown that in the same way that each numerical method has its own unique rate of kinetic energy dissipation in unsteady flows, it also has its own rate of entropy generation.

This has important ramifications in the simulation of low Mach number flows, where excess damping of flow structures leads to extremely inaccurate solutions. It is also of importance for implicit large eddy simulation. The expressions within this paper can be used to derive new variable extrapolation methods, tailored to improve the ability of Godunov methods at low Mach number flows.

Acknowledgments

The authors would like to thank Evgeniy Shapiro (Fluid Mechanics and Computational Sciences Group, Cranfield University) and Anthony Weatherhead (AWE, Aldermaston) for their advice and suggestions whilst completing the analysis, as well as Bill Rider (Sandia) for productive discussions. Ben Thornber is supported by an EPSRC-AWE PhD Case award and Dimitris Drikakis would also like to acknowledge the financial support from EPSRC, MoD and AWE through the EPSRC(EP/C515153)-JGS (No. 971) project.

Appendix A. Entropy increase in the case of an isolated velocity discontinuity

Beginning with the one-dimensional Euler equations

$$\frac{\partial \mathbf{U}}{\partial t}+\frac{\partial \mathbf{E}}{\partial x}=0, \tag{A.1}$$

where

$$\mathbf{U}=[\rho,\rho u,E]^{\mathrm{T}}, \tag{A.2}$$

$$\mathbf{E}=[\rho u,\rho u^2+p,(E+p)u]^{\mathrm{T}}, \tag{A.3}$$

$$E=\rho e+\frac{1}{2}\rho u^2, \tag{A.4}$$

$$p=\rho e(\gamma-1), \tag{A.5}$$

and ρ, e, u are the density, specific internal energy per unit volume and x-direction velocity component, respectively. Throughout this paper it is assumed that the fluid satisfies the ideal gas equation of state. The Euler equations are discretised using a first-order accurate method in time and space

$$\mathbf{U}_i^{n+1}=\mathbf{U}_i^n-v(\mathbf{E}_{i+1/2}^n-\mathbf{E}_{i-1/2}^n), \tag{A.6}$$

$$v=\frac{\Delta t}{\Delta x}. \tag{A.7}$$

Given initial conditions

$$p_{\mathrm{L}}=p_{\mathrm{R}}=p,\quad \rho_{\mathrm{L}}=\rho_{\mathrm{R}}=\rho,\quad ru_{\mathrm{L}}=\Delta u,\quad u_{\mathrm{R}}=0, \tag{A.8}$$

where the cells i and $i-1$ are in the left state, cell $i+1$ is the right state. The interface flux $\mathbf{E}_{i-1/2}^n$ is computed directly from the left hand quantities. The values of the primitive variables required to compute $\mathbf{E}_{i+1/2}^n$ are determined by solving the Riemann problem at the interface with the left and right quantities. This can be estimated with reasonable accuracy using a linearised approximation [21, p. 279]

$$p^*=p+\frac{\Delta u\rho a}{2}, \tag{A.9}$$

$$u^*=\frac{\Delta u}{2}, \tag{A.10}$$

$$\rho^*=\rho+\frac{\Delta u\rho}{2a}. \tag{A.11}$$

Thus, the conserved variables at the next time step are

$$\mathbf{U}_i^{n+1}=\begin{bmatrix}\rho\\ \rho\Delta u\\ \frac{p}{\gamma-1}+\frac{1}{2}\rho\Delta u^2\end{bmatrix}+v\begin{bmatrix}\rho\Delta u-\left(\rho+\frac{\Delta u\rho}{2a}\right)\frac{\Delta u}{2}\\ \rho\Delta u^2+p-\left(\rho+\frac{\Delta u\rho}{2a}\right)\frac{\Delta u^2}{4}-p-\frac{\Delta u\rho a}{2}\\ \left(\frac{p\gamma\Delta u}{\gamma-1}+\frac{1}{2}\rho\Delta u^3\right)-\left(\frac{\left(p+\frac{\Delta u\rho a}{2}\right)\gamma\Delta u}{2(\gamma-1)}+\left(\rho+\frac{\Delta u\rho}{2a}\right)\frac{\Delta u^3}{16}\right)\end{bmatrix}, \tag{A.12}$$

simplifying,

$$\rho^{n+1}=\rho\left(1+\frac{v\Delta u}{4}\left(2-\frac{\Delta u}{a}\right)\right), \tag{A.13}$$

$$u^{n+1}=\Delta u\frac{1+\frac{v\Delta u}{8}\left(6-\frac{\Delta u}{a}-\frac{4a}{\Delta u}\right)}{\left(1+\frac{v\Delta u}{4}\left(2-\frac{\Delta u}{a}\right)\right)}, \tag{A.14}$$

$$E^{n+1}=\frac{p}{\gamma-1}\left(1+\frac{v\gamma\Delta u}{2}\right)+\frac{1}{2}\rho\Delta u^2\left[1+\frac{v\Delta u}{16}\left(14-\frac{\Delta u}{a}-\frac{8\gamma a}{\Delta u(\gamma-1)}\right)\right]. \tag{A.15}$$

Next the pressure can be computed from $(E-1/2\rho u^2)^{n+1}(\gamma-1)$

$$p^{n+1} = \left[\frac{p}{\gamma-1}\left(1+\frac{v\gamma\Delta u}{2}\right)+\frac{1}{2}\rho\Delta u^2\left[1+\frac{v\Delta u}{16}\left(14-\frac{\Delta u}{a}-\frac{8\gamma a}{\Delta u(\gamma-1)}\right)\right]\right.$$
$$\left. - \quad \frac{1}{2}\rho\Delta u^2\frac{\left[1+\frac{v\Delta u}{8}\left(6-\frac{\Delta u}{a}-\frac{4a}{\Delta u}\right)\right]^2}{\left(1+\frac{v\Delta u}{4}\left(2-\frac{\Delta u}{a}\right)\right)}\right](\gamma-1). \tag{A.16}$$

At this point the pressure at time level $n+1$ is simplified by expanding the last term in the above equation in a binomial series, $(1+x)^{-1} \approx 1-x+x^2-\cdots$, where terms up to order Δu^2 are kept. Starting with the denominator

$$\frac{1}{1+\frac{v\Delta u}{2}-\frac{v\Delta u^2}{4a}} \approx 1-\frac{v\Delta u}{2}+\frac{v\Delta u^2}{4a}+\frac{v^2\Delta u^2}{4}+\mathcal{O}\left(\frac{\Delta u}{a}\right)^3 \approx 1, \tag{A.17}$$

multiplying out the numerator

$$\left[1+\frac{v\Delta u}{8}\left(6-\frac{\Delta u}{a}-\frac{4a}{\Delta u}\right)\right]^2 \approx 1-va+\frac{v^2a^2}{4}, \tag{A.18}$$

the pressure can now be written as

$$p^{n+1} \approx p\left[1+\frac{v\gamma\Delta u}{2}+\frac{\gamma v\Delta u^2}{8a}(2\gamma-4-va(\gamma-1))\right]. \tag{A.19}$$

For u^{n+1} and ρ^{n+1}:

$$\rho^{n+1} = \rho\left(1+\frac{v\Delta u}{2}-\frac{v\Delta u^2}{4a}\right), \tag{A.20}$$

$$u^{n+1} \approx \Delta u\left(1-\frac{va}{2}\right). \tag{A.21}$$

Setting $v = \mathcal{C}/a$ and $M = 0$ clearly gives $\lim_{M\to 0}\Delta S = 0$. In practise this limit is not reached for flows of typical interest (i.e. moving flows). The change in entropy is

$$\Delta S = \frac{R}{\gamma-1}\ln\left(\frac{p}{\rho^\gamma}\right)^{n+1} - \frac{R}{\gamma-1}\ln\left(\frac{p}{\rho^\gamma}\right)^n$$
$$\approx \frac{R}{\gamma-1}\ln\left(\frac{p\left[1+\frac{v\gamma\Delta u}{2}+\frac{\gamma v\Delta u^2}{8a}(2\gamma-4-va(\gamma-1))\right]}{\left(\rho\left(1+\frac{v\Delta u}{2}-\frac{v\Delta u^2}{4a}\right)\right)^\gamma}\right) - \frac{R}{\gamma-1}\ln\left(\frac{p}{\rho^\gamma}\right)$$
$$\approx \frac{R}{\gamma-1}\ln\left(\frac{1+\frac{v\gamma\Delta u}{2}+\frac{\gamma v\Delta u^2}{8a}(2\gamma-4-va(\gamma-1))}{\left(1+\frac{v\Delta u}{2}-\frac{v\Delta u^2}{4a}\right)^\gamma}\right). \tag{A.22}$$

Expanding the denominator in a series where

$$\frac{1}{(1+z)^m} = 1-mz+\frac{m(m+1)}{2!}z^2-\frac{m(m+1)(m+2)}{3!}z^3+\cdots, \tag{A.23}$$

$$\frac{1}{\left(1+\frac{v\Delta u}{2}-\frac{v\Delta u^2}{4a}\right)^\gamma} = 1-\frac{\gamma v\Delta u}{2}+\frac{\gamma v\Delta u^2}{4a}+\gamma(\gamma+1)\frac{v^2\Delta u^2}{8}+\mathcal{O}(\Delta u^3). \tag{A.24}$$

Multiplying this by the numerator gives

$$\frac{1+\frac{\gamma v\Delta u}{2}+\frac{\gamma v\Delta u^2}{8a}(2\gamma-4-va(\gamma-1))}{\left(1+\frac{v\Delta u}{2}-\frac{v\Delta u^2}{4a}\right)^\gamma}$$
$$\approx \left(1+\frac{\gamma v\Delta u}{2}+\frac{\gamma v\Delta u^2}{8a}(2\gamma-4-va(\gamma-1))\right)\left(1-\frac{\gamma v\Delta u}{2}+\frac{\gamma v\Delta u^2}{4a}+\gamma(\gamma+1)\frac{v^2\Delta u^2}{8}\right)$$
$$\approx 1+\frac{\gamma v\Delta u^2}{8a}[2\gamma-2+2va(1-\gamma)]. \tag{A.25}$$

Additionally, for $|\frac{\gamma v \Delta u^2}{8a}[2\gamma - 2 + 2va(1-\gamma)]| < 1$ the series expansion of the natural logarithm can be employed:

$$\ln(1+x) = x - \frac{x^2}{2} + \frac{x^3}{3}, \tag{A.26}$$

to give Eq. (39).

Appendix B. Mathematica script for first-order methods

The leading order dissipation rate at an interface where there is a jump in all primitive variables can be computed using the following script in the symbolic manipulation software Mathematica.

```
(*Initial Conditions*)
pr=p - dp/2;
pl=p+dp/2;
ur=u - du/2;
ul=u+du/2;
rr=r - dr/2;
rl=r+dr/2;

(*Star Quantities*)
ps=(pr+pl)/2+(ul - ur)r a/2;
us=(ur+ul)/2+(pl - pr)/(2 r a);
rs=rl+(ul - us) r/a;

(*Compute conservative variables at the next time step*)
ul=rl+v (rl ul - rs us)
u2=rl ul+v (rl ul^2+pl - rs us^2 - ps)
u3=pl/(g - l)+rl ul^2/2+
v ((pl g/(g - l)+rl ul^2/2) ul - (ps g/(g - l)+rs us^2/2)us)

(*Calculate primitive variables at the next times step*)
rl=Simplify[Expand[ul]]
ul=Simplify[Expand[u2/ul]]
el=Simplify[Expand[u3]]
pl=(g - l)(el - l/2 rl ul^2)

(*Calculate the entropy change and multiply by temperature*)
ln=pl/rl^g ((rl)^g/(pl));
ds=RGAS/(g - l)(ln - l);
Tds=ds a^2/(g RGAS);

(*Expand each variable in terms of the jump size to gain the leading order terms*)
TdsExp=Expand[Normal[Series[Normal[Series[Normal[Series[Tds, dp, 0, 2]],
du, 0, 2]], dr, 0, 2]]]


(*Substitute speed of sound instead of pressure p*)
TdsExp2=TdsExpl/. p -> r a^2/g
```

All that remains is to simplify the resulting expression to gain several leading order terms.

Appendix C. Mathematica script for higher order methods

This appendix details the Mathematica script used to computed the change in entropy over a single time step using van Leer extrapolation in a flow field where velocity varies, but pressure and density are locally constant.

```
(*Initial Conditions for interface i+1/2 and soln of RP using the Taylor series
expansion of the van Leer limited velocities*)
pr=P[x];
pl=P[x];
ur=U[x]+dx U'[x]/2+dx^3(U''[x]^2/8U'[x]-u'''[x]/6);
ul=U[x]+dx U'[x]/2+dx^3(-U''[x]^2/8U'[x]+u'''[x]/12);
rr=R[x];
rl=R[x];
psp=(pr+pl)/2+(ul - ur)(rr+rl) a/4;
usp=(ur+ul)/2+(pl - pr)/((rr+rl) a);
rsp=rl+(ul - usp) (rr+rl)/2/a;

(*Initial Conditions for interface i - 1/2 and soln of RP using the Taylor series
expansion of the van Leer limited velocities*)
prm=P[x];
plm=P[x];
urm=U[x]-dx U'[x]/2+dx^3(U''[x]^2/8U'[x]-u'''[x]/12);
ulm=U[x]-dx U'[x]/2+dx^3(-U''[x]^2/8U'[x]+u'''[x]/6);
rrm=R[x];
rlm=R[x];
psm=(prm+plm)/2+(ulm - urm)(rrm+rlm) a/4;
usm=(urm+ulm)/2+(plm - prm)/((rrm+rlm) a);
rsm=rlm+(ulm - usm) (rrm+rlm)/2/a;

(*Compute conservative variables at the next time step*)
ul=R[x]+v (rsm usm - rsp usp);
u2=R[x] U[x]+v (rsm usm^2+psm - rsp usp^2 - psp);
u3=P[x]/(g - 1)+R[x] U[x]^2/2+v ((psm g/(g - 1)+rsm usm^2/2)
usm - (psp g/(g - 1)+rsp usp^2/2)usp);

(*Calculate primitive variables at the next times step*)
rl=Simplify[Expand[ul]]
ul=Simplify[Expand[u2/ul]]
el=Simplify[Expand[u3]]
pl=(g - 1)(el - 1/2 rl ul^2)

(*Calculate the entropy change and multiply by temperature*)
ln=pl/rl^g ((rl)^g/(pl));
ds=RGAS/(g - 1)(ln - 1);
Tds=ds a^2/(g RGAS);


(*Substitute speed of sound instead of pressure p and substitute dt for dx, CFL and
a*) Tds2=Tds/. p -> r a^2/g; Tdsodt= Collect[Tds2/dt/. v -> dt/dx/. dt -> dx CFL/a, a];
```

To compute the entropy increase due to spatial discretisation, then it is necessary to repeat the above analysis for the exact Taylor series expansion of the cell average quantities to the cell interface and then subtract the entropy rise with the exact from the entropy rise of the van Leer interpolated method.

References

[1] H. Guillard, Recent developments in the computation of compressible low Mach number flows, Flow Turbul. Combust. 76 (2006) 363–369.
[2] E. Turkel, A. Fiterman, B. van Leer, Preconditioning and the Limit of the Compressible to the Incompressible Flow Equations for Finite Difference Schemes, John Wiley and Sons, 1994.
[3] W. Noh, Errors for calculations of strong shocks using and artificial viscosity and an artificial heat flux, J. Comput. Phys. 72 (1987) 78–120.
[4] R. Christensen, Godunov methods on a staggered mesh – an improved artificial viscosity, Tech. Rep., Lawrence Livermore National Laboratory, 1990.
[5] D. Benson, Computational methods in Lagrangian and Eulerian hydrocodes, Comput. Meth. Appl. Mech. Eng. (1992) 235–394.
[6] G. Volpe, Performance of compressible flow codes at low Mach number, AIAA J. 31 (1993) 49–56.
[7] R. Menikoff, Numerical anomalies mimicking physical effects, Tech. Rep., Los Alamos, 1995.
[8] H. Guillard, C. Viozat, On the behaviour of upwind schemes in the low Mach number limit, Comput. Fluids 28 (1999) 63–86.
[9] H. Guillard, A. Murrone, On the behaviour of upwind schemes in the low Mach number limit: II. Godunov type schemes, Comput. Fluid 33 (2004) 655–675.
[10] J. Boris, F. Grinstein, E. Oran, R. Kolbe, New insights into large eddy simulation, Fluid Dyn. Res. 10 (1992) 199–228.
[11] D. Youngs, Application of MILES to Rayleigh–Taylor and Richtmyer–Meshkov mixing, AIAA-2003-4102.
[12] A. Kolmogorov, A refinement of previous hypotheses concerning the local structure of turbulence in a viscous incompressible fluid at high Reynolds number, J. Fluid Mech. 13 (1962) 82–85.
[13] G. Naterer, Heat Transfer in Single and Multiphase Systems, CRC Press, 2003.
[14] C. Fureby, F. Grinstein, Monotonically integrated large eddy simulation of free shear flows, AIAA J. 37 (5) (1999) 544–556.
[15] A. Bejan, Entropy Generation Minimization: The Method of Thermodynamic Optimization of Finite-Time Systems and Finite-Time Processes, CRC Press, 1996.
[16] D. Youngs, Three-dimensional numerical simulation of turbulent mixing by Rayleigh–Taylor instability, Phys. Fluids A 3 (5) (1991) 1312–1320.
[17] H. Bethe, On the theory of shock waves for an arbitrary equation of state, Tech. Rep., Office of Scientific Research and Development, 1942.
[18] J. Johnson, R. Cheret (Eds.), Classic Papers in Shock Compression Science, Springer-Verlag, 1998.
[19] R. Menikoff, B. Plohr, The Riemann problem for fluid flow of real materials, Rev. Mod. Phys. 61 (1) (1989) 75–130.
[20] R. Leveque, Finite Volume Methods for Hyperbolic Problems, Cambridge University Press, 2002.
[21] E. Toro, Riemann Solvers and Numerical Methods for Fluid Dynamics, Springer-Verlag, 1997.
[22] S. Klainerman, A. Madja, Compressible and incompressible fluids, Commun. Pure Appl. Math. 33 (1982) 399–440.
[23] R. Klein, Semi-implicit extension of a Godunov-type scheme based on low Mach number asymptotics I: one-dimensional flow, J. Comput. Phys. 121 (1995) 213–237.
[24] M. Merriam, Smoothing and the second law, Comput. Method Appl. M 64 (1987) 177–193.
[25] T. Barth, Numerical methods for gasdynamic systems on unstructured meshes, in: Introduction to Recent Developments in Theory and Numerics for Conservation Laws, Springer-Verlag, 1999.
[26] H. Hugonoit, On the propagation of motion in bodies and in perfect gases in particular – II, J. de l'Ecole Polytech. 58 (1889) 1–125.
[27] B. Thornber, A. Mosedale, D. Drikakis, On the implicit large eddy simulation of homogeneous decaying turbulence, J. Comput. Phys. 226 (2007) 1902–1929.
[28] E. Garnier, M. Mossi, P. Sagaut, P. Comte, M. Deville, On the use of shock-capturing schemes for large-eddy simulation, J. Comput. Phys. 153 (1999) 273–311.
[29] C.-W. Shu, Total-variation-diminishing time discretizations, SIAM J. Sci. Stat. Comp. 9 (1988) 1073–1084.
[30] A. Jameson, Time dependent calculations using multigrid, with applications to unsteady flows past airfoils and wings, AIAA 91-1596.
[31] S. Gottlieb, C.-W. Shu, Total variation diminishing Runge–Kutta schemes, Math. Comput. 67 (221) (1998) 73–85.
[32] R. Spiteri, S. Ruuth, A class of optimal high-order strong-stability preserving time discretization methods, SIAM J. Sci. Comput. 40 (2) (2002) 469–491.
[33] B. van Leer, Towards the ultimate conservative difference scheme: IV. A new approach to numerical convection, J. Comput. Phys. 23 (1977) 276–299.
[34] D. Drikakis, W. Rider, High-Resolution Methods for Incompressible and Low-Speed Flows, Springer Verlag, 2004.
[35] F. Grinstein, L. Margolin, W. Rider (Eds.), Implicit Large Eddy Simulation: Computing Turbulent Fluid Dynamics, Cambridge University Press, 2007.